ADVANCING EARTH AND SPACE SCIENCE

JGR Oceans

Key Points:

- Tidal and storm surge energy attenuation are analyzed at different oscillation frequencies using wavelet analysis
- The research is conducted in lateral wetlands bordering Wax Lake outlet (LA). We consider signal propagating from the gulf to wetland areas
- Here, wetlands act as a low pass filter, dissipating tidal components but not the low frequency components of storm surges and hurricanes

Supporting Information:

Supporting Information may be found in the online version of this article.

Correspondence to:

G. Nordio,
nordiog@bu.edu

Author Contributions:

Formal analysis: Giovanna Nordio
Investigation: Giovanna Nordio, Sergio Fagherazzi
Methodology: Sergio Fagherazzi
Project Administration: Sergio Fagherazzi
Software: Giovanna Nordio
Supervision: Sergio Fagherazzi
Validation: Sergio Fagherazzi
Visualization: Giovanna Nordio
Writing – original draft: Giovanna Nordio
Writing – review & editing: Sergio Fagherazzi

Storm Surge and Tidal Dissipation in Deltaic Wetlands Bordering a Main Channel

Giovanna Nordio[1] ID and Sergio Fagherazzi[1] ID

[1]Department of Earth and Environment, Boston University, Boston, MA, USA

Abstract Deltas are complex systems where tidal and riverine signals interact with each other. In river-dominated deltas, where river discharge is sufficiently high, tidal amplitude is attenuated and distorted. Here we use wavelet analysis to examine the water level signal in stations located in wetlands adjacent to the main river outlet in the Wax Lake system, part of the Mississippi River Delta in Louisiana, USA. We study the signal attenuation in lateral wetlands at different frequency bands, following the propagation of the water level signal from the Gulf of Mexico to the innermost stations. During high river discharge, the astronomical tide measured inside the wetlands is reduced of 90%–98% in comparison to the tide in Atchafalaya Bay. Storm surge events, largely occurring at lower temporal frequencies, propagate conserving their energy once the signal enters the delta mouth. The river discharge signal, mostly present at frequencies lower than 1.59 μHz, is felt depending on river discharge conditions and the station position within the wetlands. Our results suggest that lateral wetlands in the Wax Lake system act as a low pass filter, attenuating tidal components but not the low frequency components of storm surges.

Plain Language Summary In this study we have analyzed the propagation of tides and storm surges in the wetlands bordering the Wax Lake outlet. The analysis is carried out with wavelets, a mathematical tool able to separate water level oscillations with different periods. We can therefore separately study tides with a period of 12 and 24 hr, and storm surges, which typically last more than one tidal cycle and have therefore a longer period. Our results suggest that the lateral wetlands of the Wax Lake Outlet attenuate tidal oscillations, but affect less storm surges with longer periods. Therefore, lateral wetlands can protect against fast changes in water level, but are less effective when a storm slowly increases the water level of the ocean.

1. Introduction

River deltas are productive ecosystems, occupying 5% of the global land area. Their high ecological value is related to the rich biodiversity and carbon stored in the soil, making them some of the most unique landscapes in the world (Künzer et al., 2014; Ottinger et al., 2013). These low-lying areas are often exposed to floods and storm surges, magnified by climate change (Kuenzer & Renaud, 2012). Many studies have focused on the importance of deltaic wetlands for attenuation of storm surge events (Leonardi et al., 2018; Möller et al., 2014; Paquier et al., 2017; Smolders et al., 2015; Stark et al., 2015; Yang et al., 2012). The loss of wetland areas is detrimental for storm surge attenuation, increasing flooding in coastal communities (Möller et al., 2014).

The morphological and hydrodynamic complexity of river deltas is related to the river-tide interactions. Fluxes of water and sediments are constantly delivered by both tides and river flow (Künzer et al., 2014; Ottinger et al., 2013). Once tides meet the river flow, they are distorted and dissipated due to bottom friction and riverine discharge (Aubrey & Speer, 1985; Cai et al., 2012, Cai Savenije, & Jiang, 2014; Godin, 1999; Jay & Flinchem, 1997; Leonardi et al., 2015; Toffolon and Savenije, 2011). The effect of river flow is similar to an increase in bottom friction, by a factor proportional to the ratio between riverine and the tidal discharge (Cai et al., 2012; Cai Savenije, & Toffolon, 2014; Leonardi et al., 2015).

Field studies of tidal propagation in marshes are very scarce (e.g., Stark et al., 2015). In particular, few studies analyzed what happens to the tidal, riverine and surge signals when they enter the wetlands bordering a large channel. A distortion of the signal can affect the wetland hydroperiod and fluxes of nutrients and sediments, thus impacting delicate wetlands ecosystems (Reed & Cahoon, 1992). Moreover, lateral wetlands can work as a buffer for storm surges, and thus be used to protect dwellings and infrastructure. The aim of this paper is to fill this knowledge gap and determine how the tidal and surge signal propagate in lateral wetlands bordering a main deltaic distributary.

Because storm surges are non-periodic, they are better studied with wavelets. Wavelets transform analysis has already been used to process signals and to quantify the river-tide-storm interactions in low-lying deltas and estuaries (Lee et al., 2018; Leonardi et al., 2015; Spicer et al., 2019). This mathematical tool can provide significant results over time-frequency and space-frequency domains, reconstructing water level signals using complex functions rather than the sinusoidal ones used in Fourier analysis (Lee & Yamamoto, 1994; Torrence and Compo, 1998).

However, wavelets have only been applied along rivers and never within wetlands. Moreover, wavelets were never applied to study large-scale surges occurring during storms and hurricanes. The second aim of this paper is to use this novel technique to quantify tidal and storm surge distortion within the wetlands bordering a main deltaic channel (Lin & Qu, 2000).

Storm and tidal inputs influence different frequency bands in the energy spectrum (Munk, 1951; Toffoli & Bitner-Gregersen, 2017). Tidal waves are generated by gravitational attraction and their periods range from 12.25 to 24.50 hr; storm surges enhance these oscillations. Storm events along with gravitation attraction generate trans-tidal waves, characterized by oscillation period higher than 24.50 hr. Finally, wind generates waves with period of seconds (Munk, 1951; Toffoli & Bitner-Gregersen, 2017). Non-tidal residual, calculated subtracting predicted water levels from observed ones, is composed of an intra-annual seasonal signal, monthly mean sea level anomalies and high-frequency residual representing storm surges driven by pressure anomalies and wind setup (Fernandez-Montblanc et al., 2019; Lee et al., 2018; Serafin et al., 2017; Spicer et al., 2019).

Spectral distribution of energy has already been studied for wind waves but not for storm surges. Jadhav et al. (2013) observed that the largest dissipation of wind-waves energy in salt marshes was near the incident spectral peak frequency, and gradually decreased for frequencies above the peak. Hansen and Reidenbach (2012) focused on the eelgrass power to reduce high frequency wave motion, allowing low-frequency waves to penetrate the submerged aquatic vegetation. Bradley and Houser (2009) similarly observed significant attenuation at high wave frequencies in the range 0.75–1 Hz. Here, we want to determine whether this low-pass filter effect also applies to storm surges and tides in deltaic wetlands.

We therefore propose an analysis of water level signals recorded by stations located in wetlands bordering the Wax Lake Outlet, a major deltaic channel of the Mississippi River delta, Louisiana USA. Two data sets, one at low river discharge and the other at high river discharge conditions, are considered. Compared to previous studies, here wavelet transform analysis is used first to identify energy inputs working at different wave frequencies, such as astronomical tide, storm surges, non-tidal residual, and river discharge. Second, the energy spectrum for different stations in the Wax Lake system is analyzed to determine the dissipation of energy at each frequency. Finally, we study the propagation of the signal among stations, shedding light on the tide-river interactions within the lateral wetlands.

2. Study Area

The Wax Lake Delta (WLD) is a river delta in the greater Mississippi River Delta (MRD), Louisiana, USA (Figures 1a–1c). The WLD is located in the Northern part of the MRD, receives water from the Mississippi River through a 40 km long "feeder channel" (Wax Lake Feeder Channel- WLFC) diverted from the Atchafalaya River, and expands in Atchafalaya Bay, in the Gulf of Mexico (Shaw et al., 2013). In 1942, the U.S. Army Corps of Engineers dredged the Wax Lake Outlet (WLO) to redirect around one-third of water of the Atchafalaya River to Atchafalaya Bay (Carle et al., 2015; Shaw et al., 2016). This project was pursued to mitigate the flooding risk in New Orleans and in the lower part of the Mississippi. WLD is the final product of the Atchafalaya River diversion. It receives between 25.6 and 38.4 Mt of sediment per year, a significant amount of which is silt and clay (Shaw et al., 2013). Recent results have estimated a WLD seaward progression of 270 m/yr between 1980 and 2002 (Shaw et al., 2013). In WLD, two types of distributary channels can be recognized. Primary channels are direct conduits from the delta apex to Atchafalaya Bay, while secondary channels connect primary channels to innermost areas, consisting of low-lying wetlands (Shaw et al., 2013). Internal channels diverging from WLO contribute to feed wetlands located north of the WLD. The stations we consider are located in this area (Figure 1c).
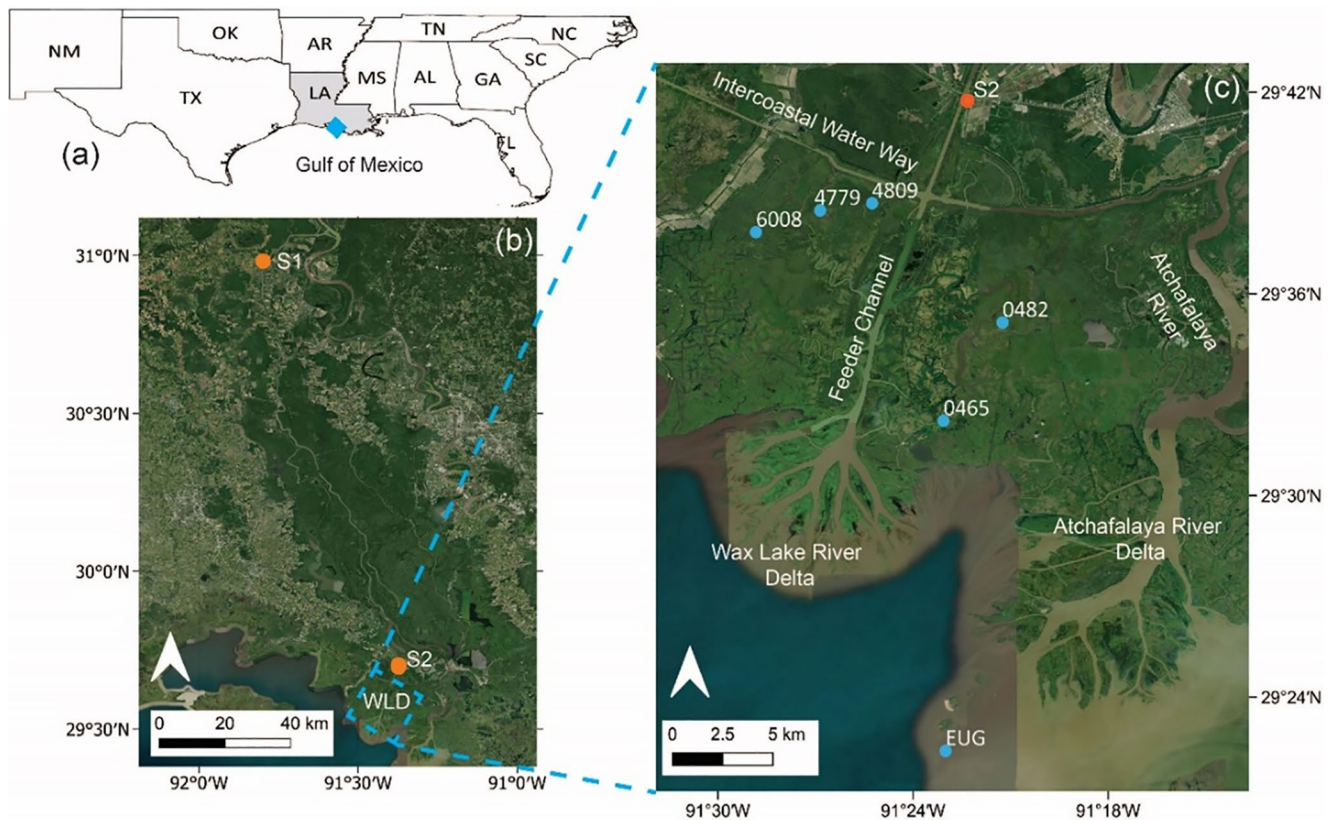
Figure 1. Study area location in the Mississippi River Delta (a). Wax Lake Delta (WLD) and USGS stations S1 and S2 (b). CRMS sites in wetland channels (0465, 0482, 6008, 4779, 4809) and NOAA station (EUG) in Atchafalaya Bay (c).

Major environmental drivers affecting water level dynamics in the MRD are river discharge, tidal fluctuations, wind waves, storms, topography, and sea-level change (Hiatt et al., 2019). WLD is strongly impacted by river discharge, that influences coastal waters through the hydrological connectivity between wetlands and river. The seasonal increase in water surface elevation in this region is mostly due to freshwater discharge coming from the Atchafalaya River and the Intercoastal Water Way (Hiatt et al., 2019). Coastal waters of Louisiana are microtidal (less than 2 m), but tidal ranges considerably vary throughout the MRD. The WLD is characterized by an average tidal range of 40 cm, with maximum tidal excursion observed during summer and winter solstices and minimum measured during spring and fall equinoxes (Hiatt et al., 2019). The tidal cycle in this region is diurnal, the most significant harmonic constituents are consequently O1 and K1. Semidiurnal constituents M2, S2 and N2 are small along the Gulf of Mexico (Hiatt et al., 2019; Marmer, 1954). Climatological forcing seems to have stronger influence than astronomical forcing in the WLD. Meteorologically induced water-level range can exceed 1 m during the winter months, when the passage of 12–24 hr storm events occurs about every 4–7 days. The amplitude of these meteorological fluctuations can be dissipated by friction when they propagate in the innermost wetland areas, where vegetation plays an important role in water level attenuation (Möller, 2006; Möller & Spencer, 2002). Hydrodynamic simulations have shown that wind stress and direction control inundation in the WLD. Between June and November, hurricanes and tropical storms affect the MRD area in an infrequent way, causing tremendous damage to coastal communities. The most recent large events were Katrina (August 2005), Rita (September 2005), Gustav and Ike (September 2008) when the surge reached 3 m above m.s.l. along the coast.

Table 1
CRMS Stations Characteristics

Station	Wetland elevation [m on NADV88]	Distance from NOAA station EUG [km]	Wetland vegetation type
0465	variable floating marsh	23.80	Fresh bulltongue
0482	0.22	32.20	Oligohaline spikerush
6008	−0.18	35.98	Swamp
4779	0.27	33.40	Swamp
4809	0.33	35.75	Swamp

3. Methods and Data

3.1. Water Levels

Five Coastwide Reference Monitoring System (CRMS) stations are chosen to study water level attenuation in wetlands (Figure 1c). The stations are situated at the end of internal channels diverging from WLO. Table 1 summarizes the characteristics of each station.

The National Oceanic and Atmospheric Association (NOAA) station 8764314 Eugene Island (EUG) located in front of the Atchafalaya Delta is considered as the reference for the water levels measured in the Gulf of Mexico. Distance between each CRMS station and the NOAA station is calculated considering the most probable and shortest pathway of water within the channel network (Table 1). Geographic Information System (GIS) and a satellite base-map provided by Environmental Systems Research Institute (ESRI) are used to measure each distance.

Two USGS stations are selected to evaluate the river effect on water levels (Figures 1b and 1c). The first station, S1 (USGS 07381490 Atchafalaya River at Simmesport), 180 km from the EUG station, is used to investigate water level frequencies associated to the river flow (Figures 2b–2d), since it is upstream of the backwater zone of 19.9 km associated to WLO (Tang et al., 2021). Here, the tidal signal is likely not felt. The second station, S2 (USGS 07381590 Wax Lake Outlet at Calumet), 25 km from the EUG station, is used to define periods of high and low river discharge (Figure 3). On average, during winter and spring the river discharge is high around 6,000 m³/s, while during summer and fall the river discharge is low around 1,400 m³/s.

Water level data in two time periods are considered to analyze attenuation under low and high river discharge conditions (Figure 2). The first period is from July to September 2017, when the river discharge is 2,000 m³/s on average (Figure 2a). The second period is from April to June 2019, when the river discharge is 7,000 m³/s on average (Figure 2c). A second water level data set from July 2019 is considered to investigate water level attenuation during Hurricane Barry. Finally, 20 storm surge events of magnitude ranging from 0.14 to 1.81 m are chosen at the EUG station from 2017 to 2020 (Table 2). For each station, the storm surge is obtained subtracting the predicted levels from the observed ones, using the T-TIDE software (Pawlowicz et al., 2002; Supporting Information S1). The storm surges at each location are summarized in Table 2.

3.2. Wavelet Transform Analysis

Water level signals characterized by tides and nonstationary components like waves, wind effects and storm surges, are particularly complex to analyze. Nonstationary components cannot be captured using simple harmonic analysis. Wavelet transform is an analysis tool well suited to study multiscale, nonstationary processes occurring over finite spatial and temporal domains. Wavelet analysis has recently attracted much attention in transient signal analysis, image analysis, communication systems and other signal processing applications (Lee & Yamamoto, 1994; Torrence & Compo, 1998). In comparison to a Fourier analysis, wavelet analysis can provide detailed information of the signal in a time-frequency space, yielding a signal decomposition at different frequencies over time. Windowed Fourier analysis can circumvent the inadequacies of simple Fourier analysis, considering a moving window analyzing the signal. The main disadvantage of windowed Fourier analysis is that the window dimension is fixed and as the frequency increases, more and more cycles in the window are needed. The strength of wavelets analysis lies in using short windows at high frequencies and long windows at low frequencies (Galli et al., 1996). Wavelet analysis deals with expansion of basic functions not in a trigonometric form, but using wavelets (Lee & Yamamoto, 1994). Wavelets are generated in forms of translation (identified by a coefficient n) and expansion (identified by a coefficient s) of fixed functions called mother functions. If the mother wavelet respects specific conditions, the wavelet transform of the real signal can be calculated. The wavelet transform can be classified as discrete or continuous depending on the working domain. In geophysics, Morlet mother wavelet is the most widely used wavelet function in a continuous domain (Lau & Weng, 1995; Lee & Yamamoto, 1994). This wavelet is complex and consists of a plane wave modified by a Gaussian envelope (Lau & Weng, 1995). The advantage of using the Morlet wavelet is its complex nature that can detect both time-dependent amplitude and
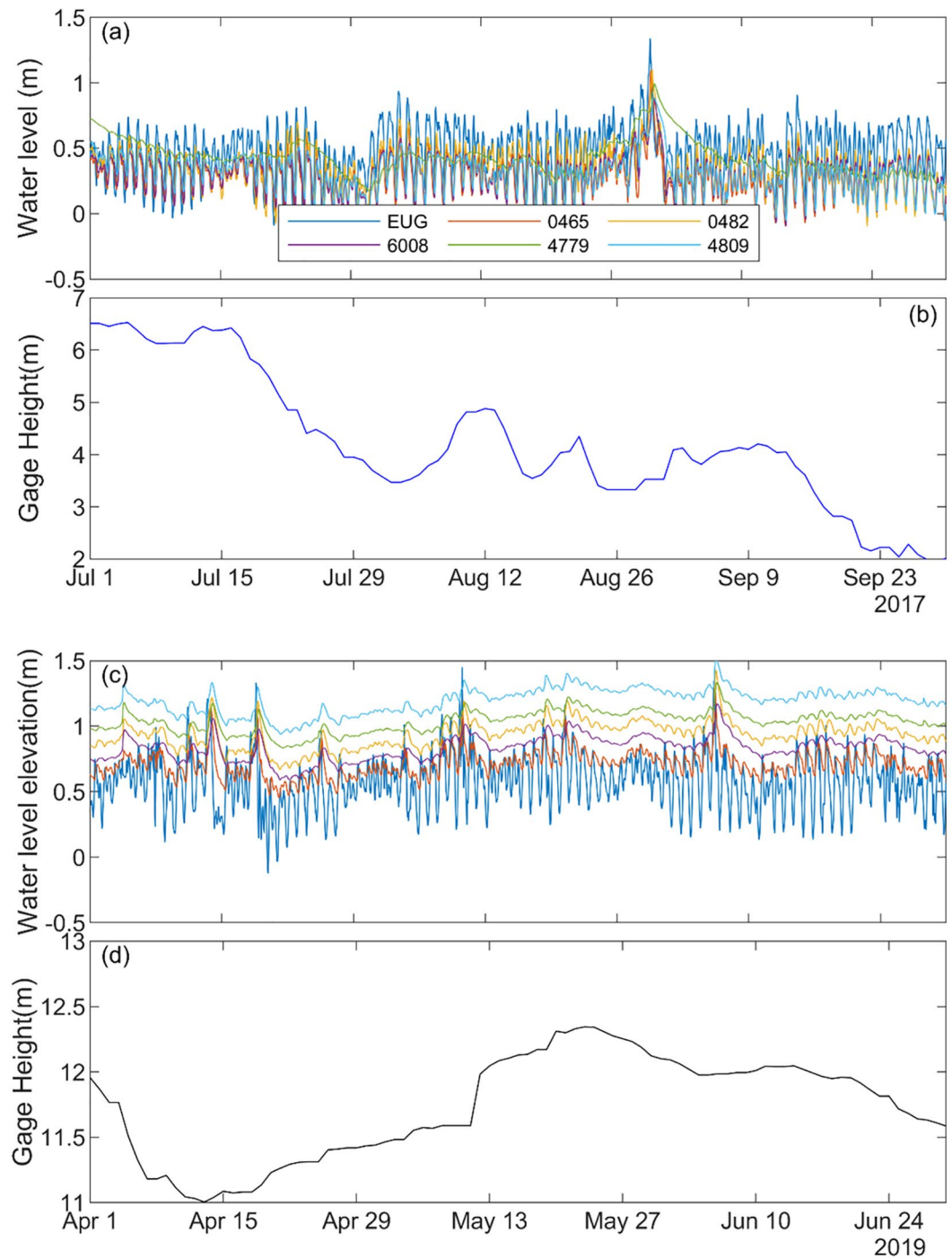
Figure 2. Water levels at different stations at low (a) and high discharge (c) (m above NAVD88). Water level in the Atchafalaya River at Simmesport station (S1) at low (b) and high discharge conditions (d).

phase for different frequencies exhibited in the time series (Lau & Weng, 1995). Because the mother wavelet is complex, also the continuous wavelet transform $w_n(s)$, is complex. The *wavelet power spectrum* can be defined as $|w_n(s)^2|$ (Flinchem & Jay, 2000; Torrence and Compo 1998). For a given signal, the power spectrum gives a plot of the portion of a signal's power (energy per unit time) falling within given frequency bins (Press et al., 1992). Here, we define signal energy as spectral energy. It can be visualized in a time-frequency plane where each point
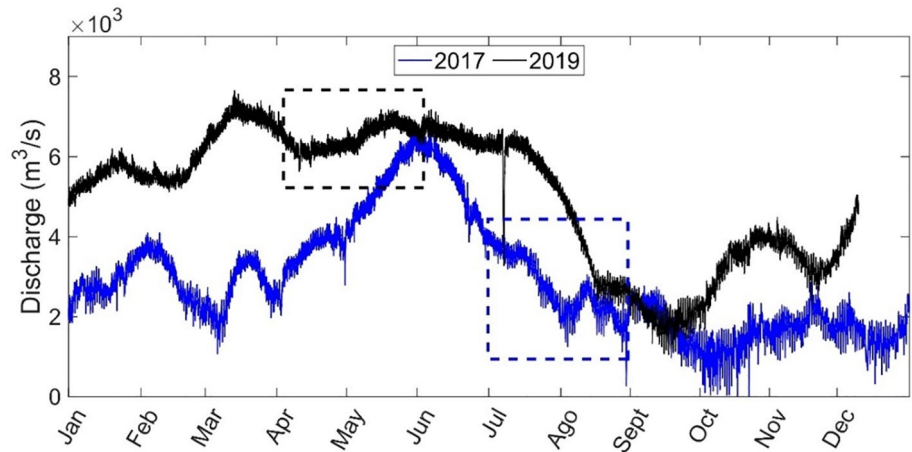
Figure 3. Discharge data at Wax Lake Outlet (Calumet station S2) in 2017 and 2019. A period of low discharge (July to September) was chosen in 2017 (blue box), while a period of high discharge (April to June) is selected in 2019 (black box).

has a specific spectral energy. Attenuation of spectral energy between two signals can be visualized in the same time-frequency plane in terms of ratio as:

$$r = \frac{|w2_i(j)^2|}{|w1_i(j)^2|}, \tag{1}$$

where $|w1_i(j)^2|$ and $|w2_i(j)^2|$ are respectively spectral energy of the first and second signal at specific time $i = 1,2…N$ and frequency $j = 1,2…S$. When the ratio is higher than 1, water level spectral energy of the second

Table 2
20 Storm Surge Events Selected From 2017 to 2020

	Time	Discharge	Water level EUG (m)	EUG (m)	0465 (m)	0482 (m)	6008 (m)	4779 (m)	4809 (m)
2017	24-Apr	Low	0.23	0.49	0.35	0.32	0.29	0.00	0.24
	12-May	Low	0.35	0.35	0.24	0.24	0.14	0.02	0.08
	29-May	High	0.59	1.03	0.35	0.18	0.03	0.02	0.05
	21-Jun	High	0.89	0.27	0.22	0.22	0.18	0.12	0.20
	22-Oct	Low	0.91	1.70	0.88	0.82	0.52	NaN	0.44
2018	5-Jun	High	0.14	0.51	0.18	0.19	0.14	0.00	0.16
	17-Jun	High	0.55	0.31	0.26	0.18	0.12	0.06	0.08
	2-Oct	Low	0.29	0.10	0.09	0.08	0.03	0.00	0.02
	11-Oct	Low	0.64	0.27	0.23	0.18	0.18	0.00	0.19
	14-Oct	Low	0.77	0.23	0.19	0.18	0.20	0.05	0.20
2019	4-Apr	High	0.57	0.35	0.04	0.10	0.07	0.01	0.03
	18-Apr	High	0.91	0.50	0.26	0.33	0.25	0.14	0.16
	6-Jun	High	0.78	0.40	0.35	0.33	0.17	0.16	0.16
	13-Jul	High	1.81	2.07	NaN	1.65	1.63	1.20	1.32
	13-Nov	Low	0.46	0.47	NaN	0.24	0.24	0.14	0.20
2020	23-Jun	High	0.67	0.55	0.20	0.12	0.08	0.04	0.10
	17-Aug	Low	0.26	0.21	0.14	0.14	0.07	0.02	0.09
	21-Sep	Low	0.98	0.20	NaN	0.13	0.15	0.05	0.15
	9-Oct	Low	1.79	1.20	NaN	0.67	0.51	NaN	0.54
	28-Oct	Low	0.68	0.51	NaN	0.35	0.12	NaN	0.13

signal is amplified compared to water level spectral energy of the first signal. Spectral energy associated to a specific frequency s can be calculated as:

$$w_s = \sum_{i=1}^{N} |w_i(s)^2|. \qquad (2)$$

Total spectral energy associated to a water level signal can be calculated as:

$$w_{tot} = \sum_{j=1}^{S} \sum_{i=1}^{N} |w_i(j)^2|. \qquad (3)$$

According to these formulas, spectral energy for each frequency band and total spectral energy are expressed in m^2.

Wavelet transform is performed using *Matlab* functions. The goal is to visualize the dominant frequencies representative of the water level signal, to recognize the astronomical and meteorological components and investigate the attenuation of the marine signals (tides and storm surges) going from Atchafalaya Bay (EUG station) to the innermost wetlands. Attenuation analysis of river signal is not provided, not having enough stations collecting data along the Atchafalaya River to Wax Lake Delta. We first apply wavelet transform analysis to CRMS and NOAA stations, decomposing the signal in a time-frequency plane. This analysis allows us to recognize storm events and tidal frequencies. We calculate the wavelet power spectrum for each station and provide a measure of spectral energy associated to single frequencies obtained by wavelet transform.

The same analysis is also applied to gage height data collected in S1, to characterize the frequencies of the river signal. In order to measure the attenuation of spectral energy at each station with respect to the spectral energy at the NOAA station (EUG), Equation (1) is used, where signal spectral energy, $w2_{n,s}$, at specific time and frequency at each CRMS station is compared to the spectral energy at EUG station, $w1_{n,s}$. The analysis is carried out considering only spectral energy values higher than $0.001 \, m^2$ at EUG station to reduce noise. This ratio provides a measure of spectral energy attenuation for each point in time and frequency. Equation (2) is instead used to estimate signal spectral energy associated to each frequency at each station. Ratio between spectral energy in wetland stations and spectral energy at station EUG is calculated for each frequency band. Signal attenuation of astronomical components derived from harmonic analysis is presented in Supporting Information S1. Equation (3) is finally used to calculate total signal spectral energy at each station. Total signal spectral energy is correlated to both distance and mean water level at each station. An additional analysis is carried out to calculate the attenuation of Hurricane Barry's signal in July 2019.

4. Results

The two data sets considered are characterized by storm surge events reaching a similar maximum water level of around 1.4 m on NAVD88 (Figures 2a and 2c). Water level oscillations are reduced going from EUG to the innermost stations, but are still present in both low and high river discharge conditions (Figures 2a and 2c). When the river discharge is high, the average water level increases inland (Figure 2c). Wavelet transform analysis at low river discharge is shown in Figure 4. Four frequency bands can be recognized. A first band with frequencies lower than 8.44 µHz, representing weekly, monthly and seasonal oscillations with a period higher than 25 hr, a second band between 8.44 and 15.74 µHz, representing tidal oscillations with period around 24 hr (the tidal harmonics K1 and O1 have frequency 11.61 and 10.76 µHz), a third band between 19.38 and 29.38 µHz representing tidal oscillations with period around 12 hr (M2, S2, and N2 have frequencies 22.37, 23.15, and 21.94 µHz, respectively) and a last band higher than 29.38 µHz, representing hourly oscillations not linked to tides. Note that because the data are collected every hour, the highest frequency that can be recorded is 140 µHz (Nyquist frequency), so that wind waves cannot be captured. In the second and third frequency bands (tidal bands) we can recognize a regular pattern repeating twice a month where spectral energy minima and maxima follow each other. This pattern is more visible in the second band (diurnal tide) and represents neap and spring modulations.

In low discharge conditions, the spectral energy in the second and third bands is lower in the wetlands, particularly at location 4779 (Figure 4). The attenuation of the tidal frequencies can be better seen in Figure 5, where we plot the ratio between the spectral energy at EUG in Atchafalaya Bay and the spectral energy at each wetland
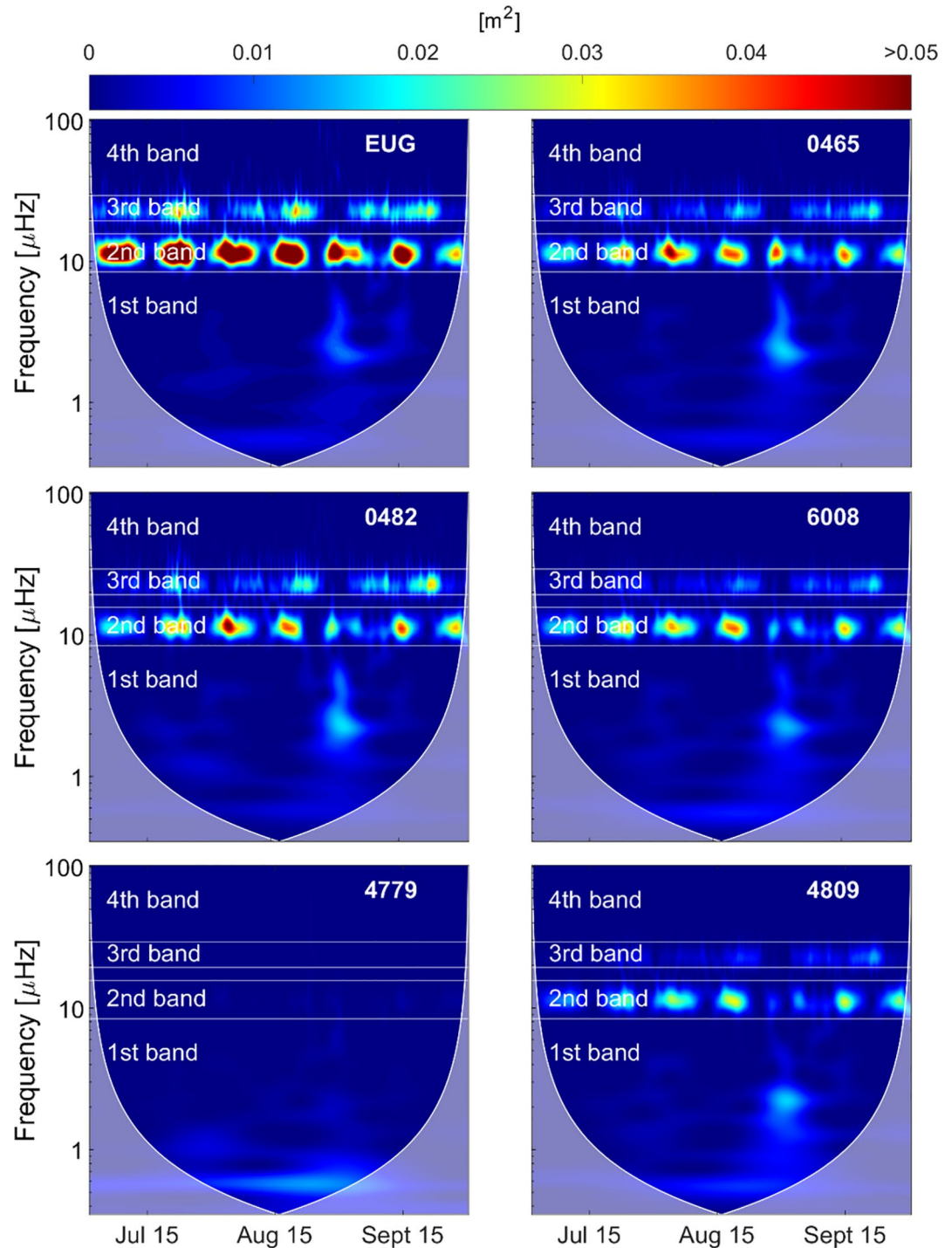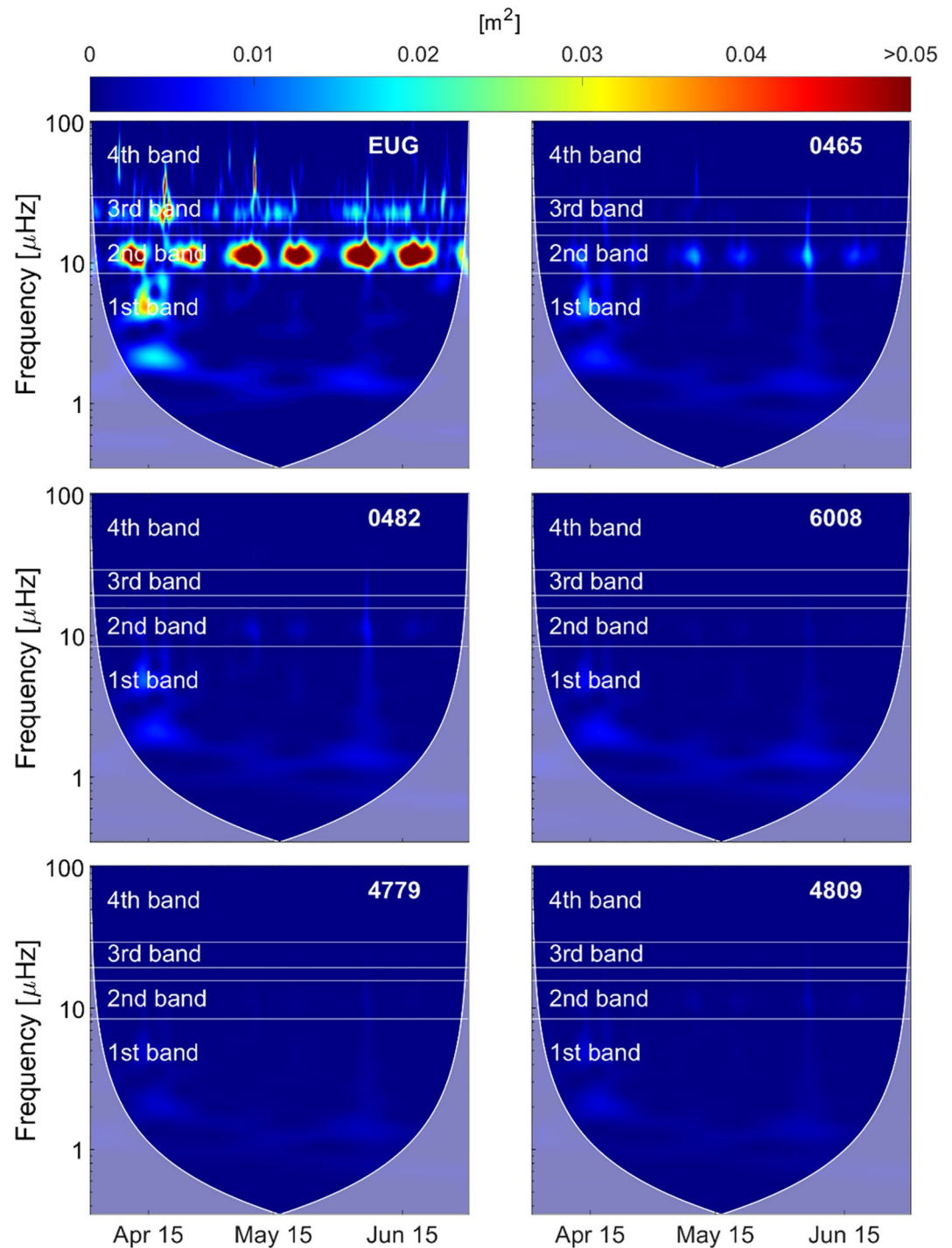
Figure 4. Wavelet power spectrum in low discharge conditions in each station. Higher energy is represented by warmer colors, while lower energy by cold colors. Cone of influence defines the valid power spectrum region.

location. In this plot we masked areas with a spectral energy below 0.001 m² at EUG. Both bands 2 and 3 are characterized by ratios below 1, indicating attenuation. The attenuation is very high at 4779, where the tidal spectral energy is basically close to zero. But considerable attenuation is also present at 4809 and 6008. Overall, the spectral energy attenuation in these bands varies from 70% to 100% (Figure 5). The colored area in the first band around August 30 represents a storm surge, with most spectral energy between frequencies 2 and 4 μHz (period between 3 and 6 days). The storm surge spectral energy is also present in the higher frequency bands. The
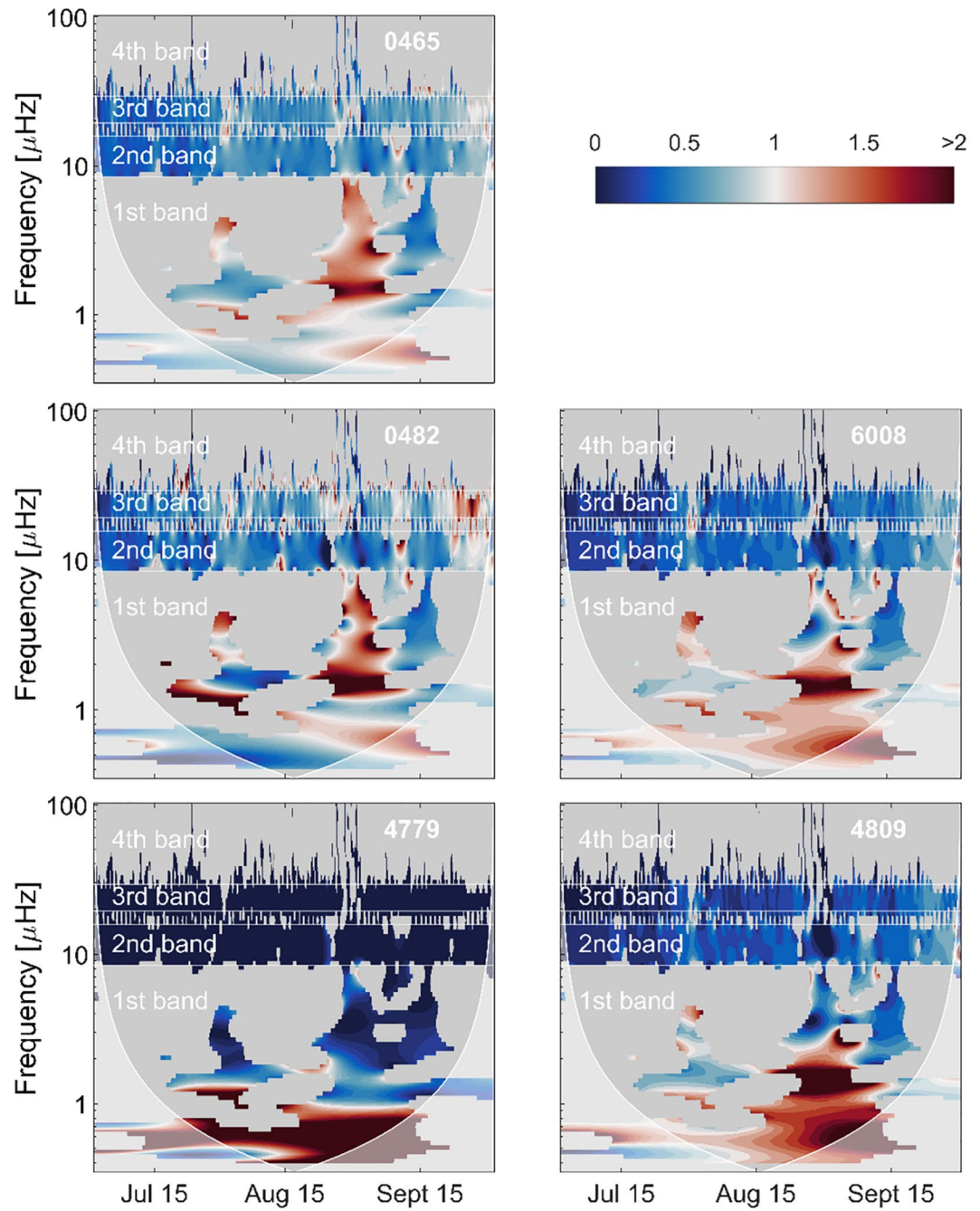
Figure 5. Ratio between spectral energy at each station and energy at the EUG station in low discharge conditions. Ratios lower than one are represented by blue colors. Gray regions are excluded from analysis. Cone of influence defines the valid power spectrum region.

spectral energy associated to this event is conserved at almost all stations (ratio close to 1 in Figure 5) except for station 4779.

Signal attenuation is more significant when river discharge is high (Figures 6 and 7). The tidal signal is barely present in the innermost stations, and the spectral energy ratios are close to zero. The attenuation is higher in the tidal bands (second and third bands) once the signal goes beyond the WLD. A complete attenuation is reached at stations 4779, 6008, and 4809. The spectral energy associated with the storm surge events in April and June 2019

Figure 6. Wavelet power spectrum in high discharge conditions in each station. Higher energy is represented by warmer colors, while lower energy by cold colors. Cone of influence defines the valid power spectrum region.

are attenuated between 30% and 70% at stations 0465 and 4809 (Figure 7). Attenuation of the astronomical signal is confirmed in the harmonic analysis (Figure S1 in Supporting Information S1).

The total spectral energy at each frequency is presented in Figures 8a and 8b. Spectral energy decreases going from station EUG to the wetland stations at frequencies higher than 1 µHz. At frequencies lower than 1 µHz, spectral energy increases in low river discharge conditions (Figure 8a). In high river discharge conditions, spectral
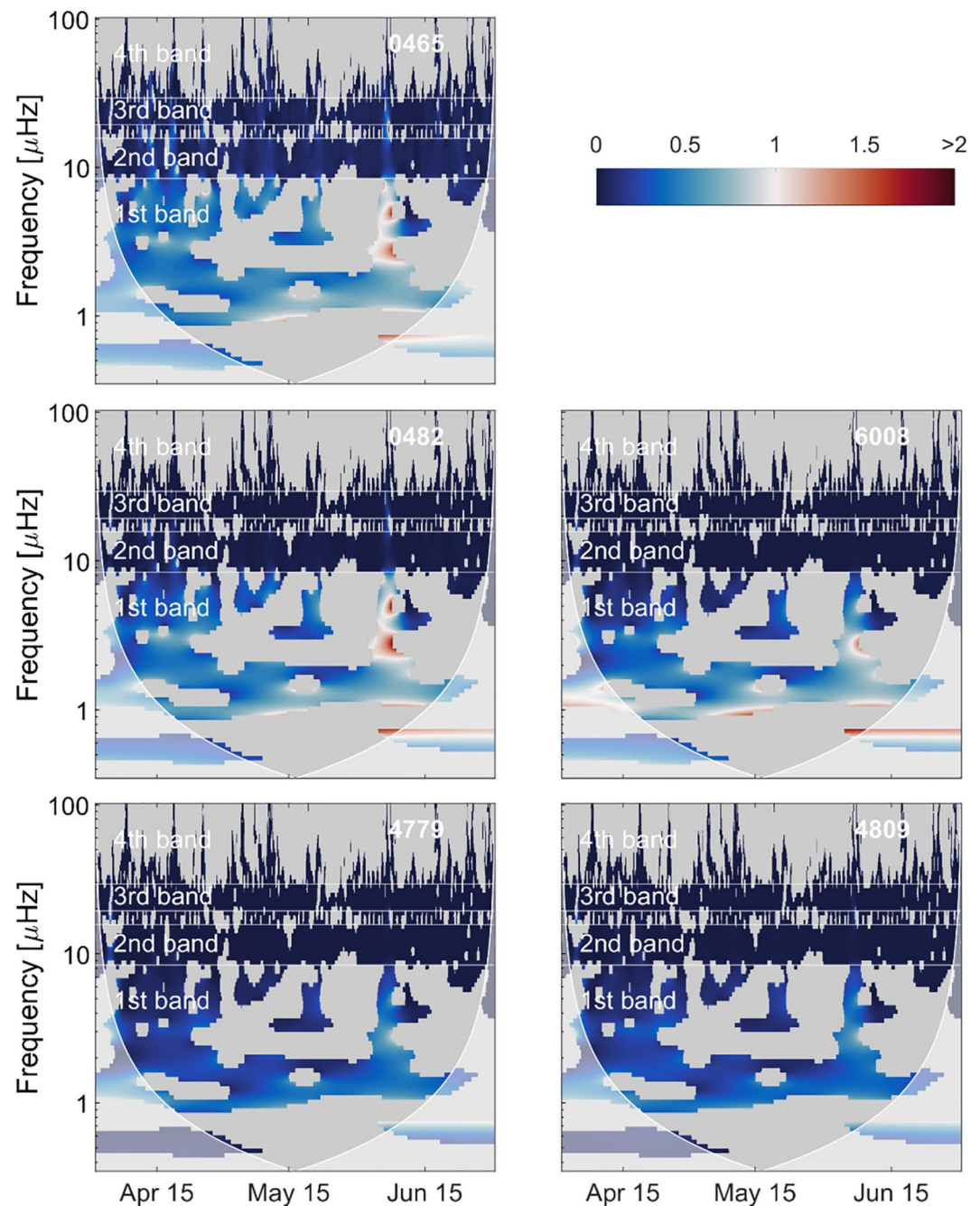
Figure 7. Ratio between spectral energy at each station and energy at the EUG station. Ratios lower than one are represented by blue colors. Gray regions are excluded from analysis. Cone of influence defines the valid power spectrum region.

energy at these frequencies attenuates as in the other frequency bands. Maximum spectral energy attenuation occurs for diurnal frequencies in both low and high discharge. In high discharge, spectral energy suddenly attenuates from values of 79 m^2 in station EUG to values of 8.3 m^2 in station 0465 (Figure 8b).

Average attenuation of the signal spectral energy for each frequency band is reported in Figures 8c and 8d. In high discharge, signal spectral energy is drastically reduced once signal enters the Wax Lake systems. In the wetland areas signal spectral energy moderately attenuates (Figure 8d). At low discharge, the dissipation ratios are higher, indicating less spectral energy dissipation. This is particularly true for the first band, displaying a spectral energy increase once signal reaches wetland stations. The increase is caused by a strong river influence at these stations.
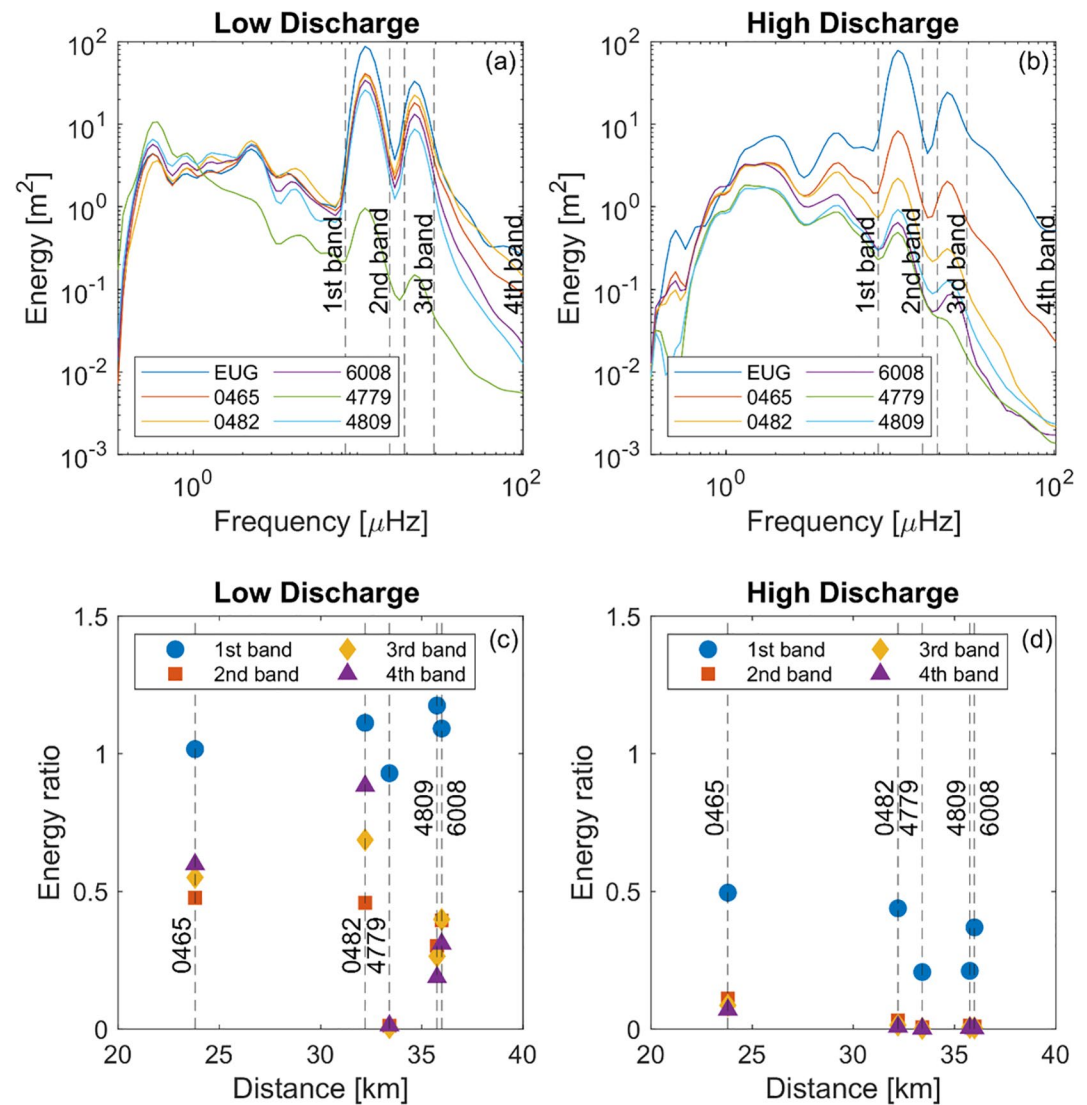
Figure 8. Total spectral energy for each frequency at each station in low discharge (a) and high discharge (b) conditions. Frequency bands are shown. Ratio between total spectral energy at each wetland station and total energy at station EUG for each band as a function of distance from station EUG in low discharge (c) and high discharge (d).

Total spectral energy of signal is related to distance of CRMS stations from EUG (Figures 9a and 9b). The spectral energy linearly decreases with distance both at low ($R^2 = 0.68$, $p < 0.05$) and high ($R^2 = 0.96$, $p < 0.05$) discharge, although at high discharge the attenuation is so strong that all the wetlands points are clustered together in Figure 9b. Diagnostic plots suggest that the higher leverage values of the EUG station could influence the final regression results. If removed, the low discharge relation become non-significant, while at high discharge it is still significant.

A power-law regression analysis only conducted on wetland points indicates a significant correlation between total signal spectral energy and mean water level ($R^2 = 0.86$, $p < 0.05$; Figure 9c). This result is more evident at high discharge, when the high water levels driven by the river dissipate most spectral energy.

The dissipation effect related to the wetlands flanking the WLO is confirmed by an additional analysis carried out using water level data collected at Calumet station (S2 in Figure 1b). Total spectral energy for each frequency band is calculated and compared to the spectral energy at the EUG station and within the wetlands (Figure 10). With this analysis, we can estimate the effect of the WLD on water level dissipation before the signal reaches the stations in the wetlands. We can suppose that the WLO does not have a significant influence on signal
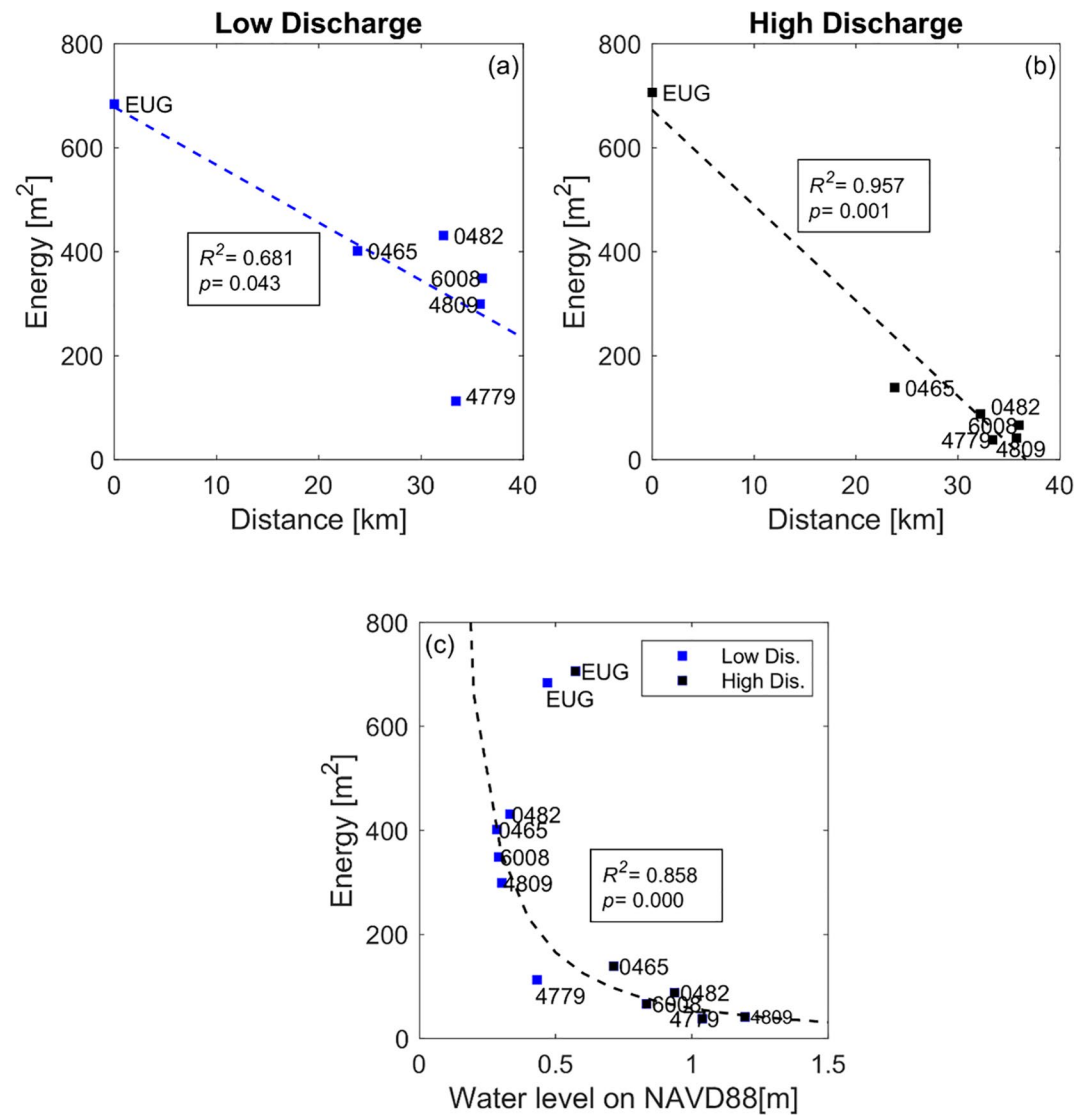
Figure 9. Total spectral energy as a function of distance from EUG station at low (a) and high discharge (b). Total spectral energy versus average water level at low (blue points) and high discharge (black points).

attenuation, because the channel is large (200 m) and deep (14 m, FitzGerald, 1998); the reduced spectral energy attenuation can be therefore ascribed to WLD. It is clear that the lateral wetlands dissipate around 50% of the signal in the higher band at low discharge and more than 90% at high discharge. The spectral energy in the first band is higher at Calumet than at EUG, because the river influence is stronger upstream.

4.1. Storm Events

Wavelet transform results are provided for the 1-month data set of July 2019, when Hurricane Berry (13 July 2019) hit the coast (Figures 11–13). On 13 July 2019 at 12.00 PM water level at station EUG reached 2.14 m. River discharge was high based on USGS data. The peak value of water level attenuated as the signal entered in the innermost stations (Figure 11). No data are available for station 0465 in this period. The spectral energy of the hurricane is mostly concentrated in the first and the second band (diurnal; Figure 11), because the storm event has a duration comparable to the diurnal timescale. The maximum attenuation occurs in the diurnal band where tidal spectral energy is present. Here, the attenuation is computed on the enhanced signal spectral energy, which also includes tidal oscillations. In the first band, between 1.59 and 8.44 μHz, spectral energy is attenuated by 40% from station EUG to station 4779 (Figure 12). Analysis performed for each frequency band confirms that
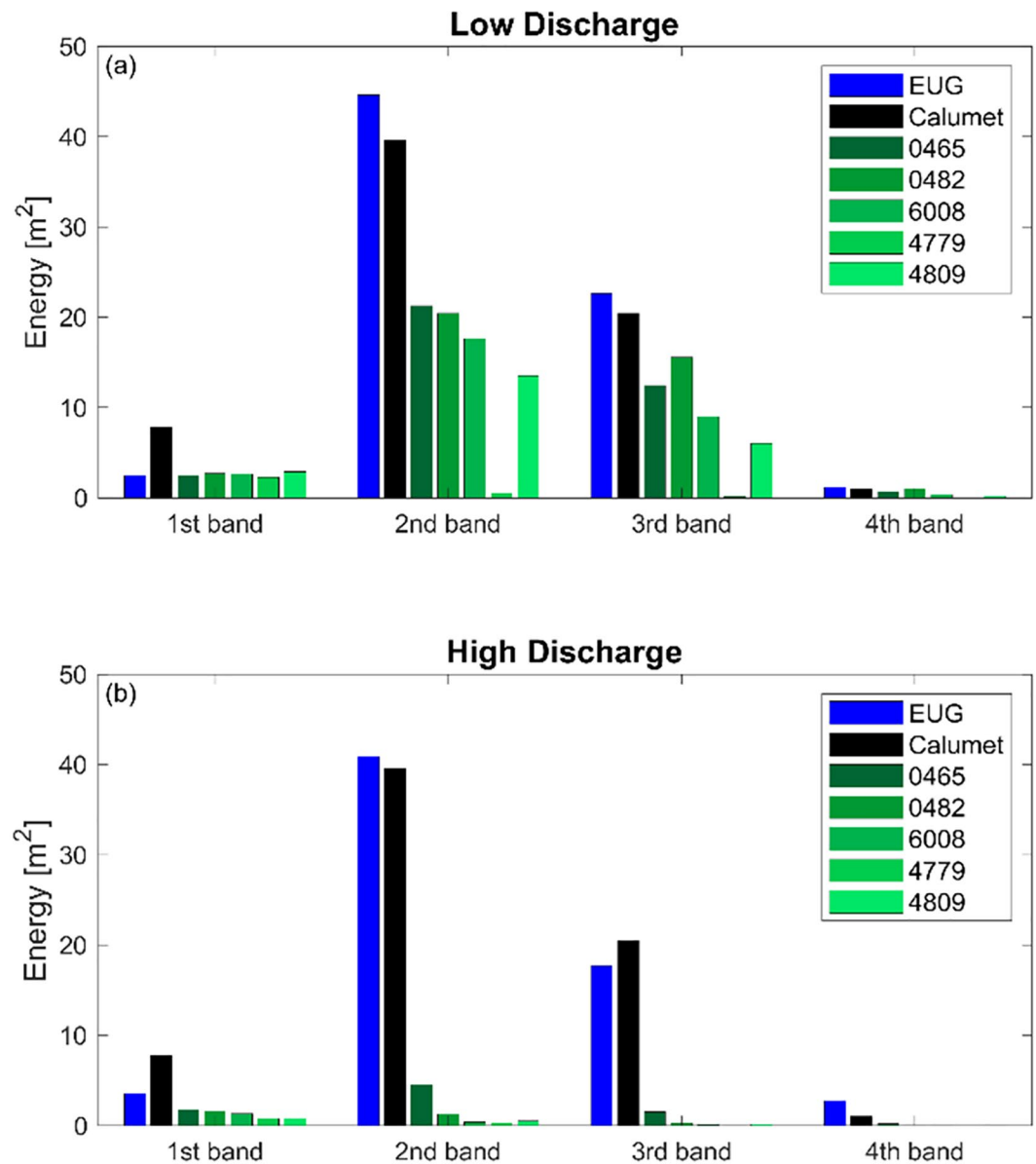
Figure 10. Spectral energy for each band at EUG station, Calumet station S2 and wetland stations in (a) low and (b) high discharge conditions.

the attenuation mostly occurred in the second, third and fourth bands (Figure 13a). Total spectral energy amount is not significantly correlated to distance from EUG station (Figure 13b).

An additional analysis was carried out considering 20 different storm events between 2017 and 2020, focusing on the non-tidal surge measured at different stations (Table 2, Figure 14). The ratios between storm-surge elevation at each wetland station and at EUG are quite different, with high standard deviation. A regression on the binned data suggests that a significant correlation between storm surge elevation and distance is present. This correlation confirms the storm surge spectral energy attenuation in the wetland interior also in terms of elevations.

4.2. River Inputs

As river discharge increases, the water levels in the wetlands are more affected by the fluvial signal. Wavelet analysis performed on the river gage data set (station S1, Figure 1) suggests that variations in river water levels
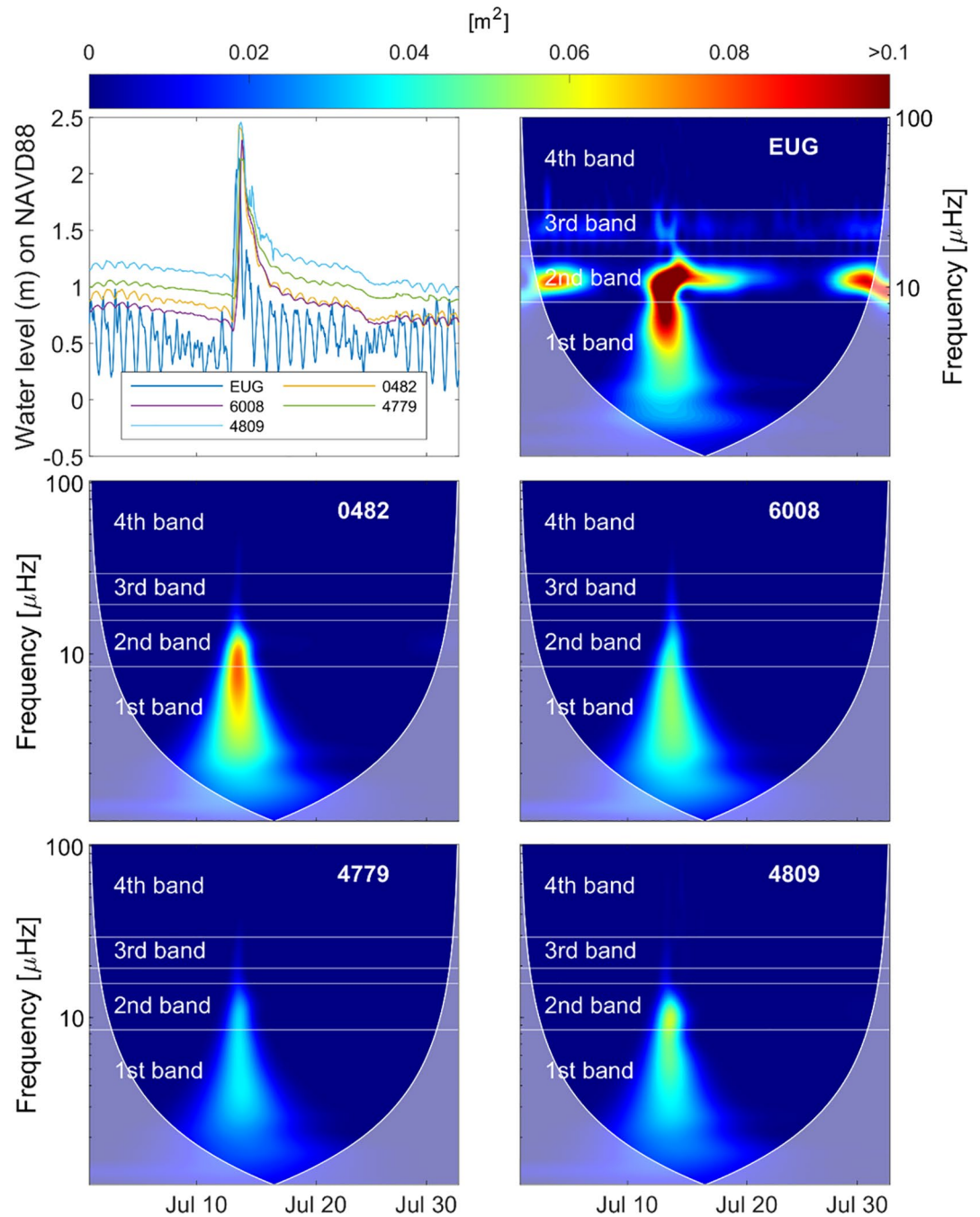
Figure 11. Signal and wavelet power spectrum in July 2019 (Hurricane Barry) in each station. Higher energy is represented by red color, while lower energy by blue color. Cone of influence define the valid power spectrum region.

mostly occur at low frequencies (<1.59 µHz; Figure 15). Water levels measured from the delta mouth to the innermost areas are affected by an amplification of the spectral energy at low frequencies in low river discharge conditions (Figures 4, 5, 8a). The amplification is higher at stations far from the mouth. For frequencies lower than 1.59 µHz in the first energy band, spectral energy associated to the matching signal increases from 0.006 m^2 at the EUG station to a maximum of 0.012 m^2 at the station 4779 (Figure 4). The significant amplification at these frequencies is likely due to the location of station 4779, in an internal channel receiving water from both WLO and IWW. Figure 9a suggests that at station 4779 the spectral energy calculated for these frequen-
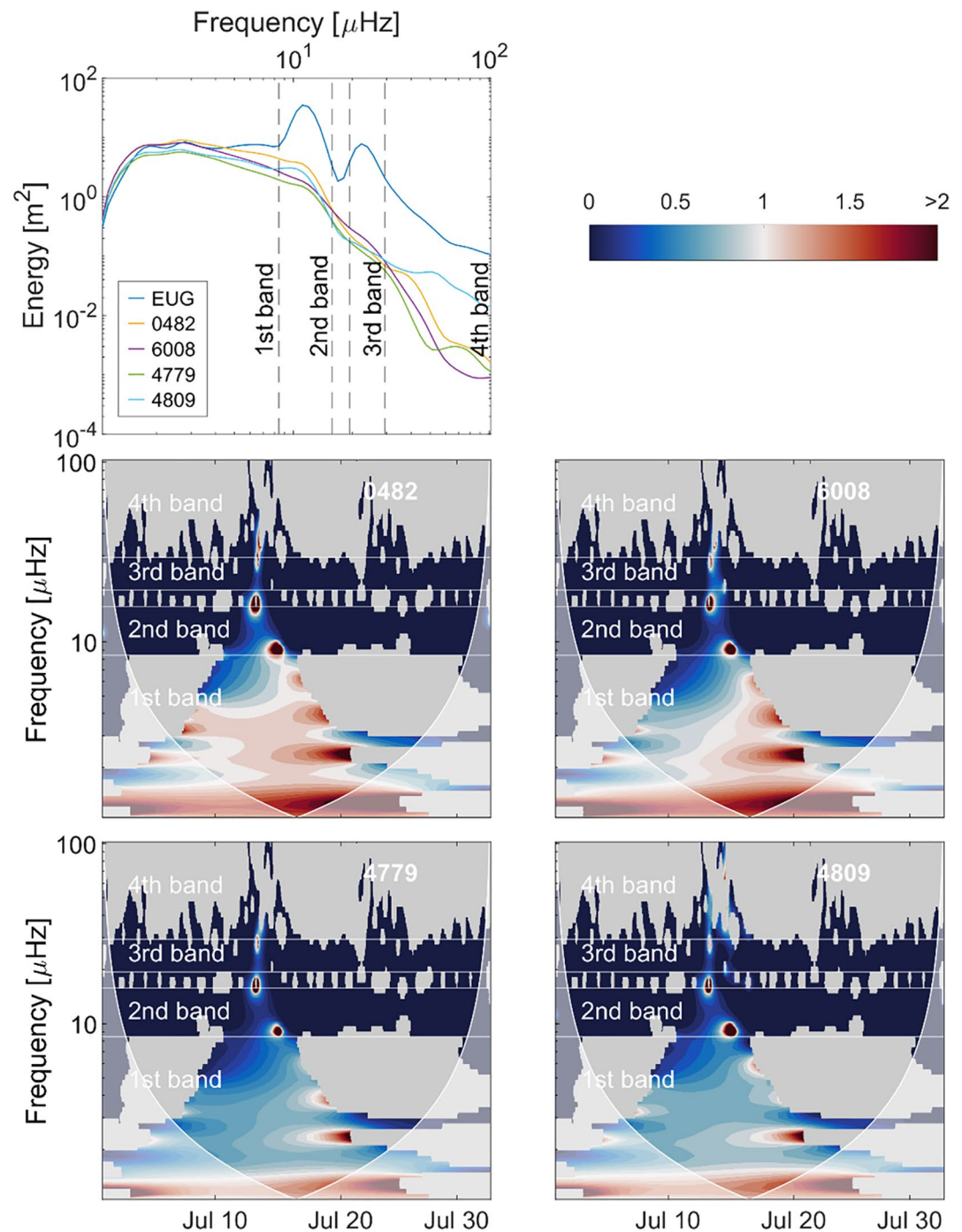
Figure 12. Ratio between energy in each station and energy in EUG station represented in a time-frequency domain using results of wavelet analysis in July 2019 (Hurricane Barry). Higher ratios are represented by red color, while lower energy by blue color. Gray regions are excluded from analysis. Cone of influence define the valid power spectrum region. Energy for each frequency is reported in the first plot.

cies (<1.59 µHz) reaches values 2 times higher (~10 m^2) than at the EUG station (~4 m^2). Therefore, stations far from the ocean are more affected by the river signal. During the high discharge period, the amplification effect due to the river is not felt (Figures 5, 6, 8b), likely because the water level in the river is almost constant (Figure 2d).
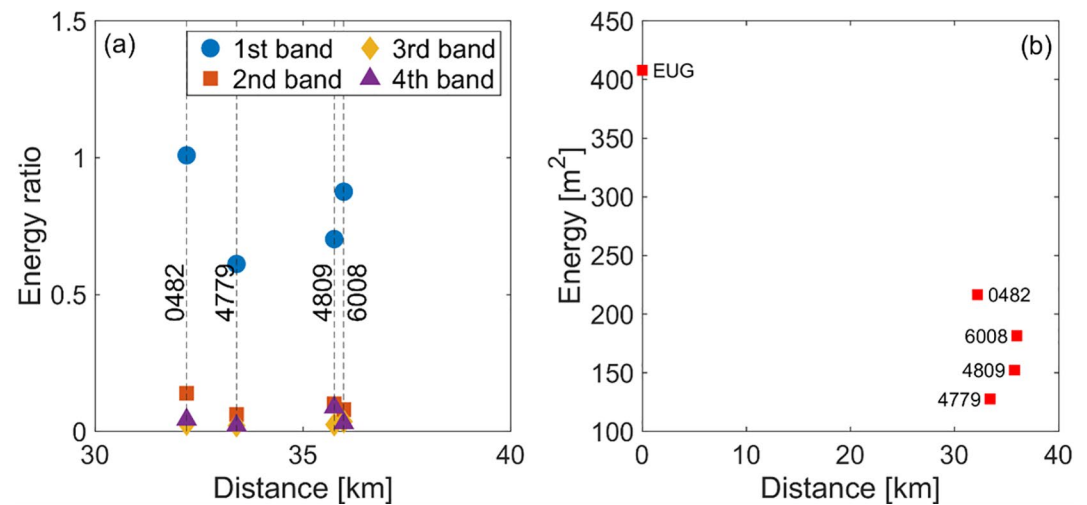
Figure 13. Variation of total energy for each band as a function of distance from EUG (a); total energy as a function of distance (b). Numbers represent CRMS stations.

5. Discussion

The water level signal varies within lateral wetlands bordering a tidal river of a major deltaic distributary. This occurs because a delta is a complex system where astronomical, storm surges and river inputs influence each other. Astronomical signal is felt in the diurnal and semidiurnal frequency bands (Wolanski & Elliott, 2015). Once the marine signal (tides and storm surges) propagates in the wetlands, the spectral energy is reduced (Figures 9a and 9b, 12b). At low discharge, the spectral energy of the astronomical signal is reduced by half when the tide reaches the first wetland station, and then it is maintained at the same level in the inner-most areas. At high discharge the attenuation is larger, leading to a 90% dissipation just in the first station closer to the main channel. Diurnal components are more attenuated. In low discharge conditions, the astronomical signal is completely dissipated at station 4779 (Figures 4 and 5). This station is directly connected to the intercoastal waterway through a small channel. As a result, the water level of the intercoastal water way might dominate over the tides.

Our results agree with previous tidal signal analyses in estuaries and embayments (Parker, 1991; Savenije, 2001). In many alluvial estuaries, the tidal damping/amplification can be well approximated by a linear relation (Savenije, 2001), as our results suggest. The role of the wetland platform is fundamental in the storm surge attenuation (Stark et al., 2015). Previous studies (Bradley & Houser, 2009; Hansen & Reidenbach, 2012; Jadhav et al., 2013) analyzed attenuation of wind waves due to vegetation. Their data indicate higher attenuation at high frequencies. Here we discovered that lateral wetlands act as a low pass filter also for tides and storm surges. In estuaries dominated by tidal action, the astronomical signal can propagate upstream (Leonardi et al., 2015; Mao et al., 2004). This occurs when river discharge is sufficiently low, and consequently there is a low damping coefficient. As river discharge increases, the water level in the river increases and the flow in the channels becomes more unidirectional. With higher water levels, the upstream propagation of tides decreases while the damping coefficient increases, causing a significant reduction in tidal amplitudes and tidal prism (Cai et al., 2012; Cai Savenije, & Jiang, 2014; Leonardi et al., 2015). Our results indicate that the same mechanism is also present in the wetlands
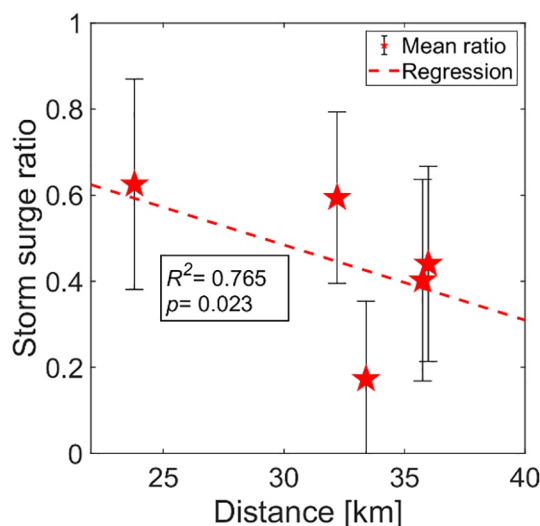

Figure 14. Ratios between storm surge elevation at each wetland station and elevation at EUG, considering storm surge events from 2017 to 2020. Mean ratios for each station are represented by red stars, and standard deviation by error bars. A significant regression line is present for the mean storm surge ratios.
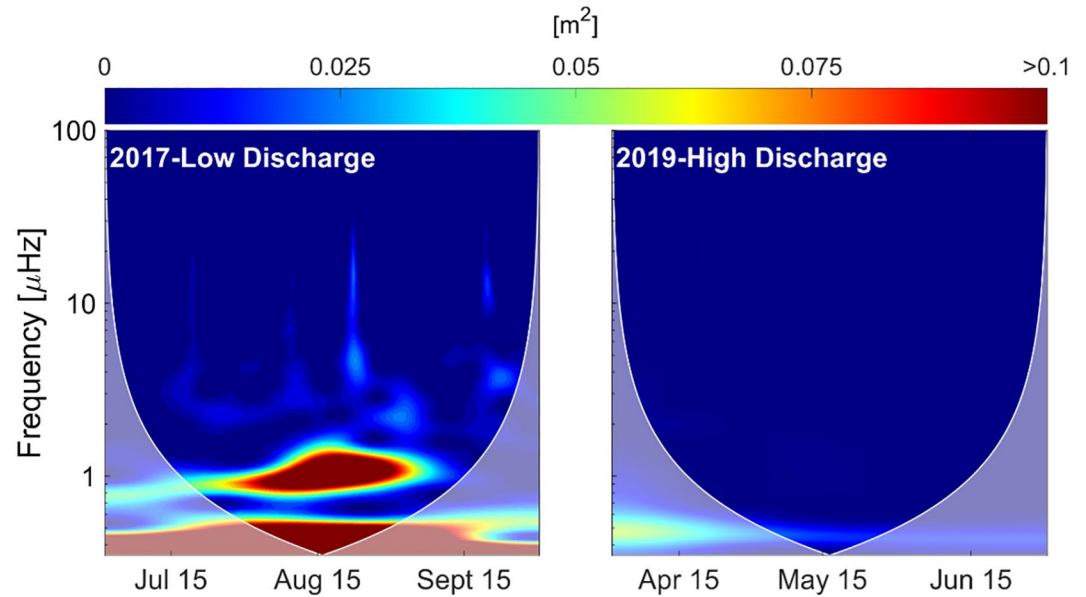
Figure 15. Wavelet power spectrum at low and high discharge conditions at the Atchafalaya River station at Simmesport (S1). Higher energy is represented by warmer color, while lower energy by cold colors. Cone of influence defines the valid power spectrum region.

bordering the tidal river or deltaic distributary. During high river flow the riverine water floods the lateral wetlands. The resulting high water levels dissipate both tides and storm surges.

Water level spectral energy measured between 1.59 and 8.44 µHz is mostly associated to meteorological events. At these frequencies trans-tidal waves can be recognized (Munk, 1951; Toffoli & Bitner-Gregersen, 2017). This spectral energy is conserved in wetland stations in low discharge conditions. At high discharge the spectral energy is progressively attenuated from station EUG to station 4779. Spectral energy at period lower than semidiurnal (fourth band) is produced by local winds and attenuates in a way similar to the spectral energy in the tidal frequencies. The analysis of Hurricane Barry yields similar results. Most hurricane spectral energy is concentrated in low frequency bands thus experiencing limited dissipation. Only the spectral energy in the tidal bands is attenuated. During the hurricane, dissipation is not related to distance from the bay computed along the tidal channels. The storm surge is so high that water can move directly on the wetland surface bypassing the channel network. The different flooding paths thus lead to different attenuation patterns.

Dissipation of tidal and storm surge signals is a well-known phenomenon. Jayne and St. Laurent (2001) mapped tidal dissipation on the rough bottom of the Earth surface. Möller et al. (2014) and Stark et al. (2015) estimated the storm surge attenuation over salt marshes in terms of reduction in water levels. Sheng et al. (2012) used numerical models to define Vegetation Dissipation Potential. Here, we estimated the attenuation of spectral energy using wavelet analysis. This method enabled us to determine the attenuation at each frequency. We find that the low frequency component of a storm surge is conserved inside the wetland areas. This is the first time that wavelet analysis is used to decompose the water level signal in wetlands.

Dissipation of tides and storm waves in wetlands is related to many factors. The volume of water that can be stored in a marsh can affect storm surge propagation, particularly when the time to fill the wetland area is shorter than the storm surge duration (Stark et al., 2015). In this case the storage area fills before the storm surge propagation stops. River input or extremely high tide conditions could significantly influence storm surge attenuation. When the storm surge signal reaches the wetland area, flooding might be already occurring. As a consequence, the storage area is reduced. Otherwise, storm water could reach these areas, sometimes not properly connected, and have difficulties to flush back before another storm surge event happens. This can justify the spread of storm surge elevation ratios in Figure 14.

Our results can be extended to other deltaic systems and, in general, to microtidal wetlands bordering large tidal channels. Tides are strongly dissipated in lateral wetlands giving rise to complex wetting and flooding patterns. This is particularly true when the river discharge is high. Variations in water levels drive fluxes of water and sediments to the wetlands (Fagherazzi et al., 2013); as a result of tidal dumping, the fluxes are more intermittent and do not follow a regular pattern, affecting vegetation. The lack of daily water level oscillations reduces subaerial periods, possibly selecting for vegetation species that can survive long hydroperiods. Reduced tidal fluxes could also diminish the input of sediments to the wetland interior, with accretion only occurring during storms or river flood events.

During a storm surge, only the tidal frequencies are dissipated, while the low frequency spectral energy (period above 25 hr) is transmitted. Lateral wetlands act therefore as a low-pass filter. The buffering effects of wetlands against storm surge inundation is therefore present only at high frequencies. However, even a reduction in tidal signal could provide some protection, since often the worst flooding events are caused by the compound effect of storm surges and high tides.

An important consequence of this findings is that while the main channel is tidally dominated, lateral wetlands are more affected by storms and wind setup. Regular water level oscillations in the main channels are replaced with more episodic events in the wetland interior. This trend is magnified during high river flow, which further dampens the tidal signal.

Our results also indicate what meteorological events are more likely filtered by lateral wetlands. A fast surge driven by a rapid, local increase in wind speed will be more dissipated. On the contrary, a long-lasting surge caused by a slow-moving storm will not be modified by the wetlands.

Unfortunately, wetlands bordering tidal rivers or deltaic distributaries have been reclaimed for dwellings and agricultural use around the world, reducing the protection they provide against storms. Our results highlight the importance of the river-wetland lateral connectivity during extreme hydrological events.

6. Conclusions

Overall tides are attenuated when traveling from large channels to the interior of lateral wetlands. At low river discharge, when the Wax Lake system is tidally dominated, the attenuation is less. At high river discharge, the tidal semi-diurnal and diurnal frequencies are dissipated of 90% once the signal reaches the first stations closer to the delta mouth. Tidal signal is not felt at stations far from the WLD mouth.

The river signal affects water levels at low frequency (<1.59 μHz). If the discharge is low, the river signal is detected at stations far from the WLD mouth. During periods with constant discharge, the river signal is not present.

Frequencies lower than 8.44 μHz are non-tidal residuals driven by storm surge events. The spectral energy at these frequencies is conserved in the lateral wetland both for small and large events (e.g., hurricanes). We conclude that the wetlands flanking WLO act as a low pass filter, dissipating tidal components but not the low frequency components of storm surges and hurricanes.

Data Availability Statement

Data supporting findings of this research are openly available in the CRMS (Coastwide Reference Monitoring System) repository at https://lacoast.gov/crms/, in the NOAA (National Oceanic and Atmospheric Association) repository at https://www.noaa.gov/ and in the USGS (United States Geological Survey) repository at https://www.usgs.gov/.

References

Aubrey, D. G., & Speer, P. E. (1985). A study of non-linear tidal propagation in shallow inlet/estuarine systems Part I: Observations. *Estuarine, Coastal and Shelf Science*, *21*(2), 185–205. https://doi.org/10.1016/0272-7714(85)90096-4

Bradley, K., & Houser, C. (2009). Relative velocity of seagrass blades: Implications for wave attenuation in low-energy environments. *Journal of Geophysical Research: Earth Surface*, *114*(F1). https://doi.org/10.1029/2007jf000951

Cai, H., Savenije, H. H., Yang, Q., Ou, S., & Lei, Y. (2012). Influence of river discharge and dredging on tidal wave propagation: Modaomen Estuary case. *Journal of Hydraulic Engineering*, *138*(10), 885–896. https://doi.org/10.1061/(asce)hy.1943-7900.0000594

Cai, H., Savenije, H. H. G., & Jiang, C. (2014). Analytical approach for predicting fresh water discharge in an estuary based on tidal water level observations. *Hydrology and Earth System Sciences*, *18*(10), 4153–4168. https://doi.org/10.5194/hess-18-4153-2014

Cai, H., Savenije, H. H. G., & Toffolon, M. (2014). Linking the river to the estuary: Influence of river discharge on tidal damping. *Hydrology and Earth System Sciences*, *18*(1), 287–304. https://doi.org/10.5194/hess-18-287-2014

Carle, M. V., Sasser, C. E., & Roberts, H. H. (2015). Accretion and vegetation community change in the Wax Lake Delta following the historic 2011 Mississippi River flood. *Journal of Coastal Research*, *31*(3), 569–587. https://doi.org/10.2112/jcoastres-d-13-00109.1

Fagherazzi, S., Wiberg, P. L., Temmerman, S., Struyf, E., Zhao, Y., & Raymond, P. A. (2013). Fluxes of water, sediments, and biogeochemical compounds in salt marshes. *Ecological Processes*, *2*(1), 1–4. https://doi.org/10.1029/ce059p0001

Fernández-Montblanc, T., Vousdoukas, M. I., Ciavola, P., Voukouvalas, E., Mentaschi, L., Breyiannis, G., et al. (2019). Towards robust pan-European storm surge forecasting. *Ocean Modelling*, *133*, 129–144.

FitzGerald, S. M. (1998). *Sand body geometry of the Wax Lake outlet delta Atchafalaya bay*. Louisiana.

Flinchem, E. P., & Jay, D. A. (2000). An introduction to wavelet transform tidal analysis methods. *Estuarine, Coastal and Shelf Science*, *51*(2), 177–200. https://doi.org/10.1006/ecss.2000.0586

Galli, A. W., Heydt, G. T., & Ribeiro, P. F. (1996). Exploring the power of wavelet analysis. *IEEE Computer Applications in Power*, *9*(4), 37–41. https://doi.org/10.1109/67.539845

Godin, G. (1999). The propagation of tides up rivers with special considerations on the Upper Saint Lawrence River. *Estuarine, Coastal and Shelf Science*, *48*(3), 307–324. https://doi.org/10.1006/ecss.1998.0422

Hansen, J. C., & Reidenbach, M. A. (2012). Wave and tidally driven flows in eelgrass beds and their effect on sediment suspension. *Marine Ecology Progress Series*, *448*, 271–287. https://doi.org/10.3354/meps09225

Hiatt, M., Snedden, G., Day, J. W., Rohli, R. V., Nyman, J. A., Lane, R., & Sharp, L. A. (2019). Drivers and impacts of water level fluctuations in the Mississippi River delta: Implications for delta restoration. *Estuarine, Coastal and Shelf Science*, *224*, 117–137. https://doi.org/10.1016/j.ecss.2019.04.020

Jadhav, R. S., Chen, Q., & Smith, J. M. (2013). Spectral distribution of wave energy dissipation by salt marsh vegetation. *Coastal Engineering*, *77*, 99–107. https://doi.org/10.1016/j.coastaleng.2013.02.013

Jay, D. A., & Flinchem, E. P. (1997). Interaction of fluctuating river flow with a barotropic tide: A demonstration of wavelet tidal analysis methods. *Journal of Geophysical Research: Oceans*, *102*(C3), 5705–5720. https://doi.org/10.1029/96jc00496

Jayne, S. R., & St Laurent, L. C. (2001). Parameterizing tidal dissipation over rough topography. *Geophysical Research Letters*, *28*(5), 811–814. https://doi.org/10.1029/2000gl012044

Kuenzer, C., & Renaud, F. G. (2012). Climate and environmental change in river deltas globally: Expected impacts, resilience, and adaptation. In *The Mekong delta system* (pp. 7–46). Springer. https://doi.org/10.1007/978-94-007-3962-8_2

Künzer, C., Ottinger, M., Liu, G., Sun, B., Baumhauer, R., & Dech, S. (2014). Earth observation-based coastal zone monitoring of the Yellow River Delta: Dynamics in China's second largest oil producing region over four decades. *Applied Geography*, *55*, 92–107.

Lau, K. M., & Weng, H. (1995). Climate signal detection using wavelet transform: How to make a time series sing. *Bulletin of the American Meteorological Society*, *76*(12), 2391–2402. https://doi.org/10.1175/1520-0477(1995)076<2391:csduwt>2.0.co;2

Lee, D. T., & Yamamoto, A. (1994). Wavelet analysis: Theory and applications. *Hewlett-Packard Journal*, *45*, 44.

Lee, M., You, Y., Kim, S., Kim, K. T., & Kim, H. S. (2018). Decomposition of water level time series of a tidal river into tide, wave and rainfall-runoff components. *Water*, *10*(11), 1568. https://doi.org/10.3390/w10111568

Leonardi, N., Kolker, A. S., & Fagherazzi, S. (2015). Interplay between river discharge and tides in a delta distributary. *Advances in Water Resources*, *80*, 69–78. https://doi.org/10.1016/j.advwatres.2015.03.005

Leonardi, N., Carnacina, I., Donatelli, C., Ganju, N. K., Plater, A. J., Schuerch, M., & Temmerman, S. (2018). Dynamic interactions between coastal storms and salt marshes: A review. *Geomorphology*, *301*, 92–107. https://doi.org/10.1016/j.geomorph.2017.11.001

Lin, J., & Qu, L. (2000). Feature extraction based on Morlet wavelet and its application for mechanical fault diagnosis. *Journal of Sound and Vibration*, *234*(1), 135–148. https://doi.org/10.1006/jsvi.2000.2864

Mao, Q., Shi, P., Yin, K., Gan, J., & Qi, Y. (2004). Tides and tidal currents in the Pearl river estuary. *Continental Shelf Research*, *24*(16), 1797–1808. https://doi.org/10.1016/j.csr.2004.06.008

Marmer, H. A. (1954). Tides and sea level in the Gulf of Mexico. *U S Fish and Wildlife Service Fishery Bulletin*, *55*(89), 101–118.

Möller, I. (2006). Quantifying saltmarsh vegetation and its effect on wave height dissipation: Results from a UK East coast saltmarsh. *Estuarine, Coastal and Shelf Science*, *69*(3–4), 337–351.

Möller, I., Kudella, M., Rupprecht, F., Spencer, T., Paul, M., Van Wesenbeeck, B. K., et al. (2014). Wave attenuation over coastal salt marshes under storm surge conditions. *Nature Geoscience*, *7*(10), 727–731.

Möller, I., & Spencer, T. (2002). Wave dissipation over macro-tidal saltmarshes: Effects of marsh edge typology and vegetation change. *Journal of Coastal Research*(36), 506–521.

Munk, W. H. (1951). *Origin and generation of waves*. Scripps Institution of Oceanography La Jolla Calif.

Ottinger, M., Kuenzer, C., Liu, G., Wang, S., & Dech, S. (2013). Monitoring land cover dynamics in the Yellow river delta from 1995 to 2010 based on Landsat 5 TM. *Applied Geography*, *44*, 53–68. https://doi.org/10.1016/j.apgeog.2013.07.003

Paquier, A. E., Haddad, J., Lawler, S., & Ferreira, C. M. (2017). Quantification of the attenuation of storm surge components by a coastal wetland of the US Mid Atlantic. *Estuaries and Coasts*, *40*(4), 930–946. https://doi.org/10.1007/s12237-016-0190-1

Parker, B. B. (Ed.), (1991). *Tidal hydrodynamics*. John Wiley & Sons.

Pawlowicz, R., Beardsley, B., & Lentz, S. (2002). Classical tidal harmonic analysis including error estimates in MATLAB using T_TIDE. *Computers & Geosciences*, *28*(8), 929–937. https://doi.org/10.1016/s0098-3004(02)00013-4

Press, W. H., Teukolsky, S. A., Flannery, B. P., & Vetterling, W. T. (1992). *Numerical recipes in Fortran 77: Volume 1: The art of scientific computing*. Cambridge University Press.

Reed, D. J., & Cahoon, D. R. (1992). The relationship between marsh surface topography, hydroperiod, and growth of Spartina alterniflora in a deteriorating Louisiana salt marsh. *Journal of Coastal Research*, 77–87.

Savenije, H. H. G. (2001). A simple analytical expression to describe tidal damping or amplification. *Journal of Hydrology*, *243*(3–4), 205–215. https://doi.org/10.1016/s0022-1694(00)00414-5

Serafin, K. A., Ruggiero, P., & Stockdon, H. F. (2017). The relative contribution of waves, tides, and nontidal residuals to extreme total water levels on US West Coast sandy beaches. *Geophysical Research Letters*, *44*(4), 1839–1847. https://doi.org/10.1002/2016gl071020

Shaw, J. B., Ayoub, F., Jones, C. E., Lamb, M. P., Holt, B., Wagner, R. W., et al. (2016). Airborne radar imaging of subaqueous channel evolution in Wax Lake Delta, Louisiana, USA. *Geophysical Research Letters*, *43*(10), 5035–5042. https://doi.org/10.1002/2016gl068770

Shaw, J. B., Mohrig, D., & Whitman, S. K. (2013). The morphology and evolution of channels on the Wax Lake Delta, Louisiana, USA. *Journal of Geophysical Research: Earth Surface*, *118*(3), 1562–1584. https://doi.org/10.1002/jgrf.20123

Sheng, Y. P., Lapetina, A., & Ma, G. (2012). The reduction of storm surge by vegetation canopies: Three-dimensional simulations. *Geophysical Research Letters*, *39*(20). https://doi.org/10.1029/2012gl053577

Smolders, S., Plancke, Y., Ides, S., Meire, P., & Temmerman, S. (2015). Role of intertidal wetlands for tidal and storm tide attenuation along a confined estuary: A model study. *Natural Hazards and Earth System Sciences*, *15*(7), 1659–1675. https://doi.org/10.5194/nhess-15-1659-2015

Spicer, P., Huguenard, K., Ross, L., & Rickard, L. N. (2019). High-frequency tide-surge-river interaction in estuaries: Causes and Implications for coastal flooding. *Journal of Geophysical Research: Oceans*, *124*(12), 9517–9530. https://doi.org/10.1029/2019jc015466

Stark, J., Van Oyen, T., Meire, P., & Temmerman, S. (2015). Observations of tidal and storm surge attenuation in a large tidal marsh. *Limnology & Oceanography*, *60*(4), 1371–1381. https://doi.org/10.1002/lno.10104

Tang, M., Xu, Y. J., Xu, W., Wang, B., & Cheng, H. (2021). Three-decadal erosion and deposition of channel bed in the Lower Atchafalaya River, the largest distributary of the Mississippi River. *Geomorphology*, *380*, 107638. https://doi.org/10.1016/j.geomorph.2021.107638

Toffoli, A., & Bitner-Gregersen, E. M. (2017). *Types of ocean surface waves, wave classification* (pp. 1–8). Encyclopedia of Maritime and Offshore Engineering. https://doi.org/10.1002/9781118476406.emoe077

Toffolon, M., & Savenije, H. H. (2011). Revisiting linearized one-dimensional tidal propagation. *Journal of Geophysical Research: Oceans*, *116*(C7). https://doi.org/10.1029/2010jc006616

Torrence, C., & Compo, G. P. (1998). A practical guide to wavelet analysis. *Bulletin of the American Meteorological Society*, *79*(1), 61–78. https://doi.org/10.1175/1520-0477(1998)079<0061:apgtwa>2.0.co;2

Wolanski, E., & Elliott, M. (2015). *Estuarine ecohydrology: An introduction*. Elsevier.

Yang, S. L., Shi, B. W., Bouma, T. J., Ysebaert, T., & Luo, X. X. (2012). Wave attenuation at a salt marsh margin: A case study of an exposed coast on the Yangtze estuary. *Estuaries and Coasts*, *35*(1), 169–182. https://doi.org/10.1007/s12237-011-9424-4